Journal of Ceramic Processing Research. Vol. 13, No. 5, pp. 517~522 (2012)

J O U R N A L O F
Ceramic Processing Research

The co-dopant concentration dependence on visible light photocatalytic efficiency in $SrTi_{1-x}Fe_{[x/2]}Cr_{[x/2]}O_3$ ($0.01 \le x \le 0.2$) perovskite photocatalysts

E. D. Jeong[a], S. M. Yu[a], J. H. Yoon[a], J. S. Bae[a], C. R. Cho[b], K. T. Lim[c], P. H. Borse[d,*] and H. G. Kim[a,*]

[a]*Busan Center, Korea Basic Science Institute, Busan 609-735, Korea.*
[b]*Department of Nano Fusion Technology, Pusan National University, Pusan 609-735, Korea*
[c]*Department of Imaging System Engineering, Pukyong National University, Busan 609-735, Korea.*
[d]*Solar H_2 PEC lab, International Advanced Research Centre for Powder Metallurgy and New Materials (ARC International), Balapur PO, Hyderabad, AP, 500 005, India.*

We studied the co-dopant (Fe-Cr) concentration dependence on the visible light photocatalytic activity of $SrTiO_3$ for the photodecomposition of gaseous iso-propyl alcohol (IPA), as well as the photo reduction of water. For the first time co-doping of perovskite $SrTiO_3$ is investigated for co-doping with Cr and Fe metal-ions at Ti substitutional site. Undoped $SrTiO_3$, Cr doped $SrTiO_3$, Fe doped $SrTiO_3$ and co-doped $SrTi_{1-x}Fe_{[x/2]}Cr_{[x]}O_4$ ($0.01 \le x \le 0.2$) were synthesized for the present study. The optimum concentration shows a maximum photodecomposition activity for IPA, as well as photocatalytic hydrogen generation under visible light ($\lambda > 420$ nm). The study on the co-dopant concentration optimization was found to be one of the important ways for fabricating an efficient photocatalyst. The optimum co-dopant concentration seems to yield a favorable density of states in the band gap of $SrTiO_3$, which otherwise may lead to recombination centers.

Key words: $SrTiO_3$, Photocatalyst, Visible light, Hydrogen.

Introduction

Titanium containing oxide *i.e.* TiO_2 is a well accepted system for various potential photocatalyst applications. Coincidently, most of the titanium-containing oxides work as potent photocatalysts, due to the role of the Ti d-orbital, and its favorable effect on the band energetics. The perovskite form of strontium titanate is one of best known systems next to TiO_2, which exhibits interesting photocatalytic properties [1-4]. $SrTiO_3$ has been a promising material for photocatalytic water splitting as well as photocatalytic oxidation reactions under UV light by virtue of its higher reduction potential and lower oxidation potential [5-9], as shown in Fig. 1. It can be observed that compared to other materials *viz*. TiO_2 and ZnO; $SrTiO_3$ is a fascinating UV active material, thus we selected $SrTiO_3$ for converting it to a visible light photocatalyst.

Visible light ($\lambda > 400$ nm) absorbing photocatalysts are desirable to utilize the useful solar spectrum for hydrogen production by splitting water, and for related applications [1]. One promising approach to develop visible light active photocatalysts is by the optical property tuning of UV light active catalysts. In the past, this has been demonstrated by anionic or cationic substitutional doping various systems of $TiO_{2-x}N_x$ [10], $TiO_{2-x}C_x$ [11], TaON [12], $SrTi_xM_{1x}O_3$ (M = Ru, Rh, Ir, Pt, Pd) [13], $Ti_{1-x}Fe_{[x/2]}Cr_{[x/2]}O_2$ [14], TiO_2 : FeC [15]. Such doping induces a red-shift in the band gap of the host lattice thereby yielding visible light active material. These materials do show stability against water, and consequent air borne reactions and thus and better than TiO_2. Recently Jang *et.al.* [9] showed that co-doping of $SrTiO_3$ displays improved optical and thus physico-chemical properties. In order to further explore the effect of the co-dopant concentration in the $SrTiO_3$ lattice, we carried out this study. In particular, we explore here the effect of the co-doping

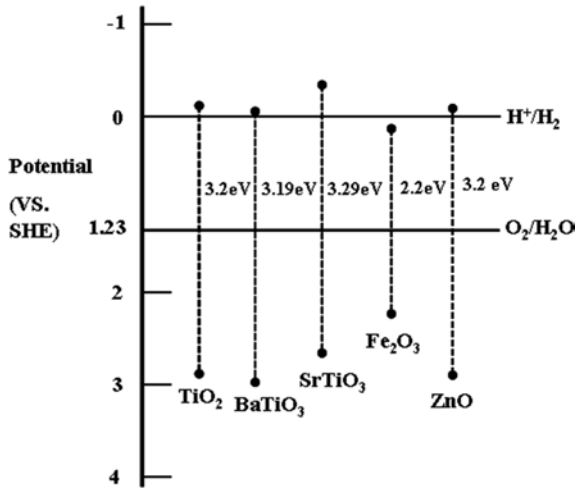

Fig. 1. Position of valence and conduction band edges for several oxide materials in contact with aqueous electrolyte at pH 0.

*Corresponding author:
Tel : +82-51-974-6104
Fax: +82-51-974-6116
E-mail: phborse@arci.res.in ; hhgkim@kbsi.re.kr

concentration on the $SrTiO_3$, photocatalytic efficiency. The concentration optimization is useful to achieve an efficient visible light photocatalyst. Consequently, we report here for the first time a co-dopant concentration optimization study in $SrTi_{1-x}Fe_{[x/2]}Cr_{[x/2]}O_3$ ($0.01 \le x \le 0.2$). The systems were synthesized by a simple solid state reaction method. We show that the optimization of the co-dopant concentration yields an efficient visible light photocatalyst, which shows a high photocatalytically generated H_2 from water as well as organic pollutant degradation under visible light irradiation ($\lambda > 420$ nm).

Experimental

$SrTi_{1-x}Fe_{[x/2]}Cr_{[x/2]}O_3$ ($0.01 \le x \le 0.2$) was synthesized by a conventional solid-state reaction (SSR) method. Stoichiometric amounts of $SrCO_3$ (99.7%, Aldrich), TiO_2 (99.99%, Aldrich), Fe_2O_3 (99%, Aldrich) and Cr_2O_3 (99.9%, Aldrich) were mixed and ground in methanol. The pelletized powders were calcined at 850-1200 °C for 5 h in a static furnace. On the other hand, for the purpose of comparison, $TiO_{2-x}N_x$ particles were also prepared by the hydrolytic synthesis method (HSM) [16], in which aqueous ammonium hydroxide solution with an ammonia content of 28-30% (99.99%, Aldrich) was slowly added drop by drop to a 20% titanium (III) chloride solution ($TiCl_3$, Kanto, contained 0.01% iron as the major impurity) for 30 minute under N_2 flow in an ice bath while continuously stirring and the suspension was stirred for 5 h to complete the reaction. After the completion of the reaction, the precipitate was filtered in air and washed several times with deionized water. The filtered powder was dried at 70 °C for 3-4 h in a convection oven. The sample obtained at this stage was an amorphous precipitated power containing ammonia and titanium. Further this sample was calcined at 400 °C for 2 h in an air flow in an electric furnace to obtain crystalline powders of $TiO_{2-x}N_x$.

The $SrTi_{1-x}Fe_{[x/2]}Cr_{[x/2]}O_3$ powders thus obtained were characterized by an X-ray diffractometer (Mac Science Co., M18XHF). X-ray diffraction (XRD) results were compared with the Joint Committee Powder Diffraction Standards (JCPDS) data for phase identification. The band gap energy and optical property of the as-prepared materials was measured by a UV-visible diffuse reflectance spectrometer (Shimadzu, UV 2401). The morphology was determined by scanning electron microscopy (SEM, Hitachi, S-2460N) and high-resolution transmission electron microscopy (HR-TEM, Philips, CM 200). The electronic-structure calculation of $SrTi_{1-x}Fe_{[x/2]}Cr_{[x/2]}O_3$ was based on the FP-LAPW (full-potential linearized augmented plane wave) method, which used the generalized gradient approximation within the density functional theory, known to be an efficient and accurate scheme for solving any electron problems for a crystal. The Wien97 package was used in this study. The crystallographic parameters including lattice parameters and atomic positions were adopted from the literature for the calculation [17].

The photo-reduction of water was carried out at room temperature in an upper-irradiation type Pyrex reaction vessel hooked up into a closed gas circulation system. Photocatalytic reduction was carried out by irradiating suspended powders using a Hg-arc lamp (500 W) equipped with a cutoff filter ($\lambda \ge 420$ nm). The H_2 evolution was examined in an aqueous methanol solution (distilled water 80 ml and CH_3OH 20 ml) by stirring 0.3 g of the catalyst loaded with 0.2 wt% Pt. Before photocatalytic reactions, all the catalysts were loaded with 0.2 wt% Pt using a conventional impregnation method using aqueous $PtCl_2$. The concentration of the reaction product (H_2) was determined by a gas chromatograph equipped with a thermal conductivity detector (a molecular sieve 5-Å column and Ar carrier). For all the samples, the photocatalytic degradation of iso-propyl alcohol (IPA) was studied to estimate the photocatalytic activities under visible-light irradiation ($\lambda \ge 420$ nm). About 200 ppm of gaseous iso-propyl alcohol (IPA) was injected into a 500-ml Pyrex reaction cell filled with air and 0.3 g of the catalyst. The concentration of the reaction products (CO_2) was determined using a gas chromatograph equipped with a thermal conductivity detector (TCD) and CTR 1 packed column. Before the reactions, 0.2 wt% of Pt was deposited on the photocatalysts by using the photo-deposition method under visible light ($\lambda \ge 420$ nm).

Results

Figure 2 display the XRD spectra of $SrTiO_3$ and doped - $SrTi_{1-x}Fe_{[x/2]}Cr_{[x/2]}O_3$ ($0.01 \le x \le 0.2$) systems. All the samples exhibited the original cubic $SrTiO_3$ structure for a dopant concentration with $x < 0.2$. However, within the given concentration range there was significant shift in the 110 plane due to the introduction of Cr and Fe ions at the substitutional Ti sites of the $SrTiO_3$ lattice, thereby validating the doping in the perovskite system. This fact is further confirmed by the respective changes in the UV-DRS spectra of the doped photocatalysts. Fig. 3 shows the UV-DRS spectra of $SrTi_{1-x}Fe_{[x/2]}Cr_{[x/2]}O_3$ system. It clearly indicates that with an increase in the co-doping concentration from $x = 0.05$ to 0.1, the respective spectra show a trend of an increase in absorbance in the region marked by the dotted circle. It is also important to mention that the bandgap of co-doped samples showed a reduction with reference to the band gap of $SrTiO_3$ [13] thereby making the samples useful to absorb the visible light photons. The band gaps estimated from the DRS spectra are shown in Table-1. Thus the co-doped samples showed a systematic variation in visible light absorption with the variation of

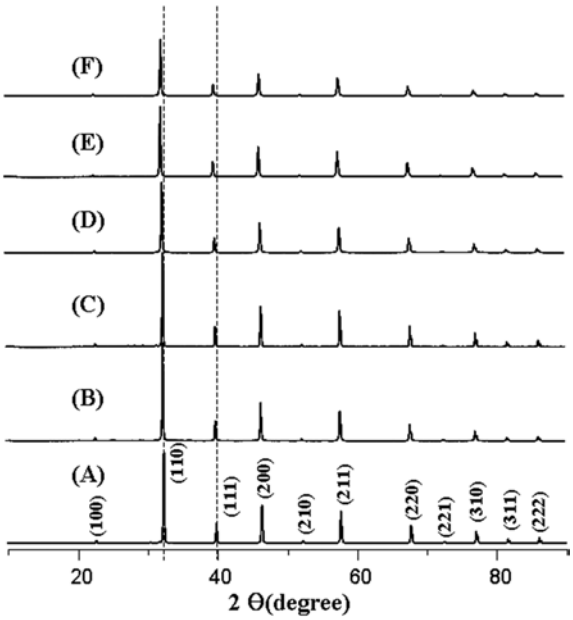

Fig. 2. X-ray diffraction patterns of undoped and doped $SrTiO_3$ photocatalysts viz. (a) : $SrTiO_3$; (b) : $SrTi_{0.99}Fe_{0.005}Cr_{0.005}O_3$; (c) : $SrTi_{0.97}Fe_{0.015}Cr_{0.015}O_3$; (d) : $SrTi_{0.95}Fe_{0.025}Cr_{0.025}O_3$; (e) : $SrTi_{0.9}Fe_{0.05}Cr_{0.05}O_3$; (f) : $SrTi_{0.8}Fe_{0.1}Cr_{0.1}O_3$; The dotted lines indicate the doping-induced shift in the diffraction angle for the 110 and 111 planes.

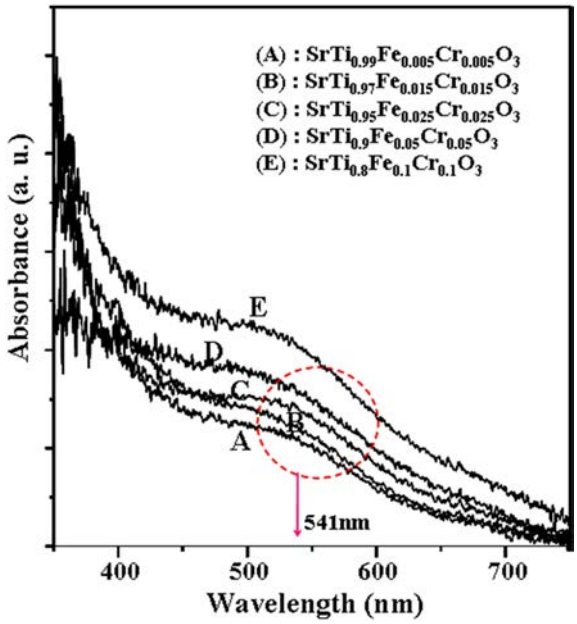

Fig. 3. UV-vis diffuse reflectance spectra of Cr-Fe co-doped $SrTiO_3$ samples.

co-dopant concentration in $SrTi_{1-x}Fe_{[x/2]}Cr_{[x/2]}O_3$ system.

To evaluate the photocatalytic activities of these $SrTi_{1-x}Fe_{[x/2]}Cr_{[x/2]}O_3$ ($0.01 \le x \le 0.2$) materials, their visible light photocatalytic hydrogen production was analyzed and compared with a titanium oxynitride sample. Table-1 shows the estimated photocatalytic H_2 gas evolved over various systems along with their corresponding band gaps as estimated from the DRS studies. These samples were loaded with Pt and further used for photocatalytic H_2 production from a methanol-water solution under visible light irradiation ($\lambda \ge 420$ nm). For the sake of simplicity the detailed result on the Pt concentration optimization is presented in a later section, however in this section we are referring to Pt loaded samples unless otherwise stated. Fig. 4, shows a SEM and TEM micrograph of typical $SrTi_{0.95}Fe_{0.025}Cr_{0.025}O_3$ sample indicating that Pt can be detected over the surface of the base photocatalyst. As shown in Table-1, the co-doped samples showed significant enhancement in H_2 generation, other samples showed no or a trace amount of H_2 evolution. This indicates that an optimum Cr-Fe concentration (*i.e.* $x = 0.025$) is necessary to obtain maximum H_2

Table 1. Photocatalytic H_2 production from a mathanol-water solution for various photocatalysts. Pt (0.2 wt%) loaded in all photocatalysts.

Catalyst	Energy band gap		H_2 evolution (mmol/gcat.hr)		
			UV light light	Visible light	Visible
	E_g(eV)-1	E_g(eV)-2	irradiation ($\lambda > 210$ mm)	irradiation ($\lambda > 420$ mm)	irradiation QY
$SrTiO_3$	3.25	-	122	0	0
$SrTi_{0.93}Cr_{0.03}O_3$	3.25	2.00	78	38	0.9
$SrTi_{0.93}Fe_{0.03}O_3$	3.25	2.48	57	12	0.2
$SrTi_{0.99}Fe_{0.005}Cr_{0.005}O_3$	3.25	2.29	134	47	1.1
$SrTi_{0.97}Fe_{0.015}Cr_{0.015}O_3$	3.25	2.29	148	56	1.3
$SrTi_{0.95}Fe_{0.025}Cr_{0.025}O_3$	3.25	2.29	177	92	2.1
$SrTi_{0.9}Fe_{0.05}Cr_{0.05}O_3$	3.25	2.29	161	51	1.2
$SrTi_{0.8}Fe_{0.1}Cr_{0.1}O_3$	3.25	2.29	92	Trace	-
$TiO_{2-x}N_x$	3.2	2.73	11	Trace	-

Pt (0.2 wt%) loaded in all materials, 0.3 g. Light source: 450-W ace lamp (Oriel) with UV cutoff filter ($\lambda \ge 420$ mm). Reaction was perfomed in an aqueous methanol solution (methanol 20 ml + distilled water 80 ml). (a) The wavelength axis for a tangent line drawn on the absorption spectrum.

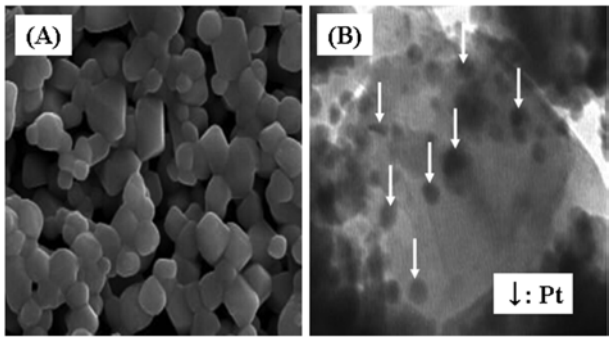

Fig. 4. Typical images of (A) SEM; and (B) TEM of a 0.2 wt% platinum-loaded $SrTi_{0.95}Fe_{0.025}Cr_{0.025}O_3$ photocatalyst.

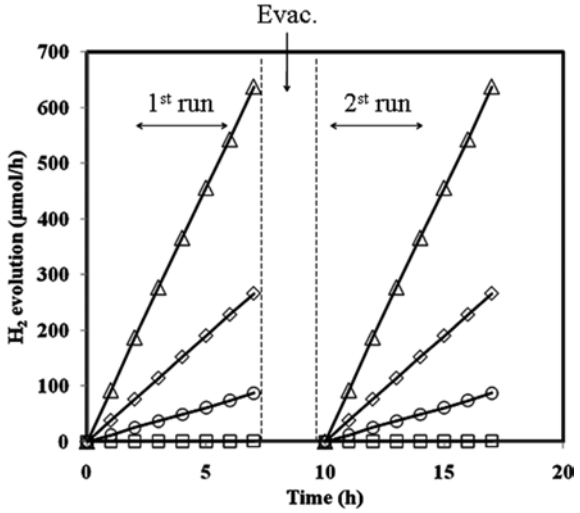

Fig. 5. Time course of H_2 gas evolution from △ $SrTi_{0.95}Fe_{0.025}Cr_{0.025}O_3$, ◇ $SrTi_{0.93}Cr_{0.03}O_3$, ○ $SrTi_{0.93}Fe_{0.03}O_3$, □ $TiO_{2-x}N_x$ under visible light irradiation in an aqueous solution by stirring 0.1 g of catalyst loaded with Pt (0.2 wt%). The reaction system was evacuated every 6 h in order to remove gaseous products from the gas phase.

evolution. The photocatalyst stability and time dependent H_2 evolution can be seen in Fig. 5. The figure clearly demonstrates the photocatalytic hydrogen generation over $SrTi_{1-x}Fe_{[x/2]}Cr_{[x/2]}O_3$ $(0.01 \le x \le 0.2)$ systems. The evolution rate increased with reaction time, the H_2 evolved regained after evacuation of the reactor reaction indicating the photocatalytic nature of the reaction.

Photocatalytic quantum yield (QY) of the photocatalyst is an important parameter to understand and compare the efficacy of a photocatalyst system. It can be calculated using the following equation [18-19]:

$$QY = H_2 \text{ evolution rate}/12.639 \times [(I_1-I_3)-(I_1-I_2)] \times A_1/A_2 \times 100 \quad (1)$$

where I_1 is the blank light intensity, I_2 is the scattered light intensity, I_3 is the photocatalyst light intensity, A_1 is the illuminated area of the photo reactor, A_2 is the area of the sensor face, and 12.639 is the mole number of photons with $\lambda \ge 420$ nm emitted from the light source for 1 h. Photocatalytic QY calculations indicate

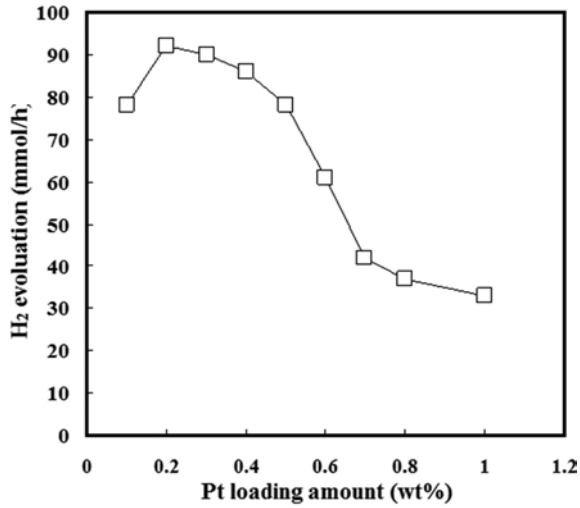

Fig. 6. Graph showing the effect of Pt-loading concentration (in $SrTi_{0.9}Fe_{0.025}Cr_{0.025}O_3$) on the hydrogen production, under visible light irradiation ($\lambda \ge 420$ nm).

that co-doped samples always performed better than singly (Cr or Fe) doped and updoped $SrTiO_3$ systems as shown in Table 1. The $SrTi_{1-0.95}Fe_{0.025}Cr_{0.025}O_3$ sample showed a maximum QY ~ 2.1% in contrast to the zero value of $SrTiO_3$. The QYs of the other samples (except $SrTi_{0.8}Fe_{0.1}Cr_{0.1}O_3$ and $TiO_{2-x}N_x$, those showed a trace showed lower QY values than 2.1%, but not a zero value like that of the host lattice. This is an important achievement of the present study.

Further, we investigated the dependence of the visible light photocatalytic activity on the amount of Pt loading on a $SrTi_{0.9}Fe_{0.025}Cr_{0.025}O_3$ sample. The photocatalytic activity showed a maximum activity at 0.2 Pt wt% and then gradually decreased for other amounts of Pt loading as shown in Fig. 6. Thus, this indicates that an optimum level of Pt loading on $SrTi_{0.9}Fe_{0.025}Cr_{0.025}O_3$ is responsible for a further enhancement in hydrogen production. Fig. 6, demonstrates the Pt loading over $SrTiO_3$ particle surfaces as seen in HRTEM (see Fig. 4(b)). It is clear that Pt islands adhere over the base $SrTiO_3$ photocatalyst. It is important to mention here that Pt-loading plays a vital role of a co-catalyst thereby favoring the electron-hole charge separation during the photocatalytic reaction. The concentration dependent efficiency can be correlated to the optimum Pt-concentration. This indicates that a low Pt is not sufficient to take part in the photocatalytic reaction, whereas at a high concentration the metallic species act as electron trapping centers thus reducing the efficiency of photocatalytic reduction.

Thus, irrespective of the co-catalyst role, an efficient photocatalytic behavior of the samples can be attributed mainly to two factors, [1] the co-doping which renders higher visible light absorptivity to samples as observed in Fig. 3; [2] The optimum concentration of Cr-Fe, which otherwise possibly leads to certain unfavorable defect states thereby leading to

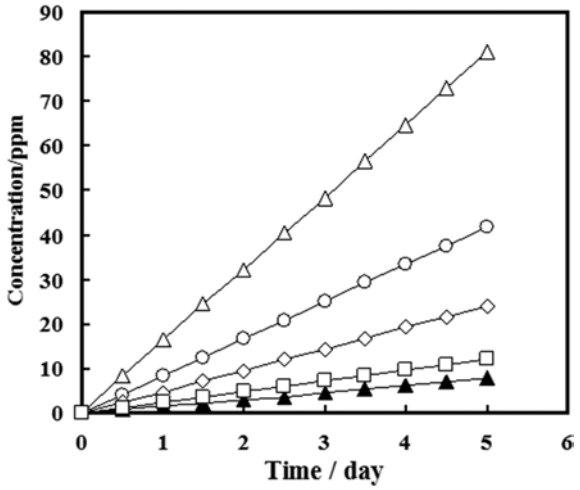

Fig. 7. Time courses of CO_2 evolution from IPA decomposition over different materials under visible light irradiation ($\lambda \geq 420$ nm). [Photocatalyst, 0.3 g; IPA concentration, 200 ppm in air.] for *viz.* ◇ $SrTi_{0.93}Cr_{0.03}O_3$, □ $SrTi_{0.93}Fe_{0.03}O_3$, ○ $SrTi_{0.97}Fe_{0.015}Cr_{0.015}O_3$, △ : $SrTi_{0.95}Fe_{0.025}Cr_{0.025}O_3$, ▲ $TiO_{2-x}N_x$.

unnecessary recombination losses.

In order to explore the photocatalytic application of these samples in gaseous systems, we analyzed their photocatalytic activities under visible light ($\lambda > 420$ nm), for oxidative decomposition of gaseous IPA. Fig. 7 shows the time courses of CO_2 evolution from IPA decomposition over singly (Cr or Fe) doped $SrTiO_3$, $SrTi_{1-x}Fe_{[x/2]}Cr_{[x/2]}O_3$ (for $x \sim 0.015$, 0.025) and $TiO_{2-x}N_x$ samples. Doped, co-doped $SrTiO_3$ and oxynitride samples showed significant activity. Interestingly, Cr-Fe co-doped $SrTiO_3$ showed the highest activity. In each case the concentration of CO_2 increased rapidly with increasing irradiation time. The activity of Fe-doped $SrTiO_3$ was very similar to that for $TiO_{2-x}N_x$ but not better than Cr-doped $SrTiO_3$. The Cr and Fe co-doped $SrTiO_3$ showed much higher decomposition rates and activities than those of singly (Cr or Fe only) doped TiO_2. Thus, the co-doped samples exhibited approximately two times higher photocatalytic activity for photodecomposition of IPA gases than others under visible light. This clearly demonstrates that the optimum Cr-Fe concentration is very important to achieve the best photodecomposition performance.

Discussion

The favorable effect of the co-dopants on the photocatalytic performance was further analyzed. In order to understand this, it is desirable to look at the electronic structure of the base photocatalyst. Fig. 8 shows the total density of states (DOS) of the cubic $SrTiO_3$ structure computed using FLAPW formalism under density functional theory. It can be seen from the present theoretical electronic structure calculations that the band gap is constituted due to a contribution of O 2p orbitals (for the valence band) and Ti 3d orbitals

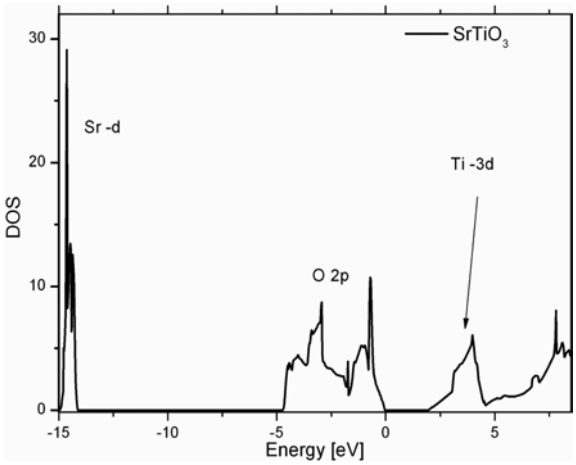

Fig. 8. The total density of states (DOS) of the perovskite $SrTiO_3$ structure computed using FLAPW formalism under density functional theory.

(the conduction band). The main purpose of the DOS calculation was to understand the valence and conduction band of the host lattice of $SrTiO_3$. Hence an in-depth DOS study [13] of the doped system is beyond the scope of this paper. Thus we have only studied and presented the DOS results of the host lattice, and utilized the information for related discussion. To elaborate further, we utilize the DRS results presented in Fig. 3. The band structures of the Fe/Cr doped and co-doped $SrTiO_3$ are mainly affected by the 3d band states of these transition metal ions (Cr^{3+} and Fe^{3+}). The DRS studies do validate the point by inducing respective absorptions bands, below the main $SrTiO_3$ absorption edge. Thus, it indicates that the partially filled Fe/ Cr 3*d* band are located below the conduction band. Depending on the above investigation, we propose schematic diagram for the co-doped system. Fig. 9 displays the flat band potential values, and schematic representation proposed to explain the photocatalytic behavior of the co-doped system and N doped TiO_2. Accordingly, when large wavelengths photons ($\lambda > 420$ nm) were used for illumination, only the electrons in the Cr 3*d* and Fe 3*d* interband, instead of electrons in the valence band of $SrTiO_3$, were excited to the conduction band. In turn, Cr^{3+} and Fe^{3+} lose electron to become Cr^{4+} and Fe^{4+}. Such photo-excitation of electrons is not possible in the $SrTiO_3$ system, because the energy of the incident light is much less than its band gap energy. In contrast, N-TiO_2, being comparatively a greater band gap material absorbs less visible light photons. Further, in the oxynitride the N states above the valence band of TiO_2 are not as useful in yielding high photocatalytic activity as in co-doped $SrTiO_3$. Consequently, the co-doped $SrTiO_3$ absorb more visible light photons than the oxynitride photocatalyst. Such a lower band gap facilitates easy generation of holes [1]. These holes can react with water to produce the highly reactive OH. Both the holes and the OH exhibit a strong oxidation

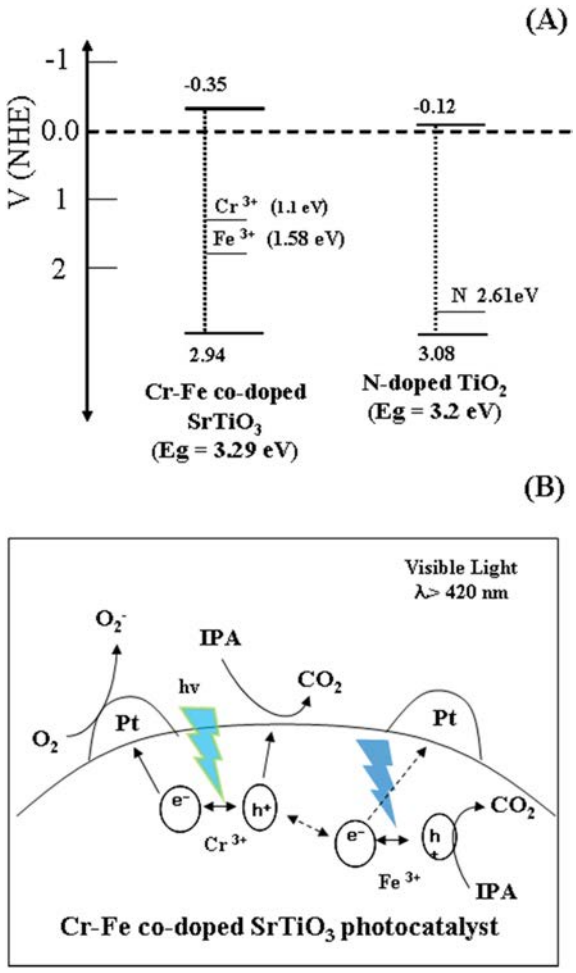

Fig. 9. (A) The bandgap position of Cr-Fe co-doped $SrTiO_3$ and $TiO_{2-x}N_x$ photocatalysts; (B) A schematic describing the mechanism for photocatalytic decomposition of gaseous isopropyl alcohol.

potential for the degradation of organic compounds. Thus the above discussion provides a guideline to explain the role of Cr- and Fe- co-doped $SrTiO_3$ in yielding better performance as a visible light photocatalyst.

Conclusions

In order to develop efficient visible light photocatalysts, transition metals co-doped $SrTiO_3$ were synthesized by simple solid state reaction. The co-doping effect was analyzed in the context to the photo-reduction of water as well as IPA photodegradation. The Cr - Fe doping concentration was varied in $SrTi_{1-x}Fe_{[x/2]}Cr_{[x/2]}O_3$ ($0.01 \le x \le 0.2$) systems. These systems exhibited 2-4 times higher photocatalytic activities for H_2 production, than did the individually (Cr/Fe) doped $SrTiO_3$ system under visible light irradiation ($\lambda > 420$ nm). The $SrTi_{0.9}Fe_{0.025}Cr_{0.025}O_3$ sample shows the highest photocatalytic activity for water reduction as well as for IPA decomposition. The activity is mainly attributed to (i) optimum Cr - Fe concentration; and (ii) the larger absorption around 550 nm wavelength in the co-doped system than in the singly doped $SrTiO_3$ system.

Acknowledgement

The authors acknowledge the support of KBSI grant (T30320, C31223), Hydrogen Energy R&D Center, Korea. One of the authors (PB) acknowledges the support of Director ARCI, (DST lab) Hyderabad, India.

References

1. Fujishima, K. Hashimoto and T. Watanabe, TiO_2 Photocatalysis: Fundamentals and Applications, BKC Inc., Tokyo (1999).
2. Pramod H. Borse, C.R. Cho, K.T. Lim, J.S. Bae, E.D. Jeong, T.E. Hong, H.J. Kim and H.G. Kim, J. Ceram. Pro. Res. 12 (2011) 592-598.
3. J.S. Jang, S.H. Choi, H.G. Kim and J.S. Lee, J Phys. Chem. C 112 (2008)17200-17205.
4. S.W. Bae, P.H. Borse, S.J. Hong, J.S. Jang, J.S. Lee, E.D. Jeong, T.E. Hong, J.H. Yoon, J.S. Jin, H.G. Kim. J. Korean Phys. Soc. 51 (2007) S22-S26.
5. K.Momen, A. Kudo and T. Onichi, J. Phys. Chem. 90 (1986) 292-295.
6. S. Ahuja and T.R.N. Kutty, J. Photochem. Photobiol. A, Chem. 97 (1996) 99-107.
7. K.I. Shimizu, S. Itoh, T. Hatamachi, T. Kodama, M.Sato and K. Toda, Chem. Mater. 17 (2005) 5161-5166.
8. W. Choi, A. Termin, M.R. Hoffmann, Angew. Chem. Int. Ed. Engl. 33 (1994) 1091-1092.
9. J.S. Jang, J.S. Lee, P.H. Borse, K.T. Lim, O.S. Jung, E.D. Jeong, M.S. Won and H.G. Kim. J. Korean Phys. Soc. 55 (2009) 2470-2475.
10. R. Asahi, T. Ohwaki, K. Aoki, Y. Taga, Science, 293 (2001) 269-271.
11. S.U.M. Khan, M. Al-Shahry and W.B. Jr. Ingler, Science 297 (2002) 2243-2245.
12. G. Hitoki, T. Takata, J. Kondo, M. Hara, H. Kobayashi, and K. Domen, Chem. Commun. (2002) 1698-1699.
13. S.W. Bae, P.H. Borse, J.S. Lee, Appl. Phys. Lett. 92 (2008) 104107.
14. E.D. Jeong, Pramod H. Borse, J.S. Jang, J.S. Lee, O.S. Jung, H. Chang, J.S. Jin, M.S. Won and H.G. Kim, J. Ceram. Pro. Res. 9 (2008) 250-253.
15. Thi Quynh Hoa, Nguyen, Zonghoon Lee, and Eui-Tae Kim, J. Electrochem. Soc. 159 (2012) K42-K45.
16. J.S. Jang, H.G. Kim, S.M. Ji, S.W. Bae, J.H. Jung, B.H. Shon, J.S. Lee, J. Solid State Chem. 179 (2006) 1067-1075.
17. D.W. Hwang, H.G. Kim, J.S. Lee, J. Kim, W. Li and S.H. Oh, J. Phys. Chem. B 109, (2005) 2093-2102.
18. S.M. Ji, P.H. Borse, H.G. Kim, J.S. Jang, S.W. Bae, and J.S. Lee, Phys. Chem. Chem. Phys., 7 (2005) 1315-1321.
19. S.J. Hong, P.H. Borse, S.M. Ji, J.S. Jang, J.S. Lee, E.D. Jeong, H.G. Kim, H.K. Park, J. Korean Phys. Soc. 51 (2007) S27-S31.